

Gate-tunable superconducting quantum interference devices of PbS nanowires

Hong-Seok Kim¹, Bum-Kyu Kim¹, Yiming Yang², Xingyue Peng², Soon-Gul Lee¹, Dong Yu², Yong-Joo Doh^{1,*}

¹*Department of Applied Physics, Korea University Sejong Campus, Sejong, 339-700, Republic of Korea*

²*Department of Physics, University of California, Davis, CA 95616, USA*

*E-mail: yjdoh@korea.ac.kr

Abstract

We report on the fabrication and electrical transport properties of gate-tunable superconducting quantum interference devices (SQUIDs), made of semiconducting PbS nanowire contacted with PbIn superconducting electrodes. Applied with a magnetic field perpendicular to the plane of the nano-hybrid SQUID, periodic oscillations of the critical current due to the flux quantization in SQUID are observed up to $T = 4.0$ K. Nonsinusoidal current-phase relationship is obtained as a function of temperature and gate voltage, which is consistent with a short and diffusive junction model.

Nano-hybrid superconducting junctions,¹⁻² made of a single-crystalline nanostructure contacted with conventional superconductors, provide a useful tool to explore the combined effects of quantum electrical transport in nanostructure and superconducting phase coherence. Supercurrent transistors, in which the superconducting coupling through the nanostructure is gate-tunable, have been developed using semiconductor nanowires (NWs),^{1, 3} carbon nanotube,⁴ and graphene⁵. Controlled Cooper pair splitters for nonlocal entanglement have also been realized using the nanostructures.⁶⁻⁷ Furthermore, recent studies on the gate-tunable macroscopic quantum tunneling⁸⁻⁹ and Majorana bound states¹⁰⁻¹¹ in the nano-hybrid superconducting junctions would pave the way for developing nano-hybrid superconducting qubits.¹²⁻¹³

A superconducting quantum interference device (SQUID),¹⁴ formed with two superconducting junctions connected in parallel, is used as a very sensitive magnetometer and a key building block for a superconducting flux qubit¹⁵ as well. So far, nano-hybrid SQUIDs have been made of various nanostructures such as NWs,¹⁶ carbon nanotube,¹⁷ and graphene.¹⁸ Very low operation temperatures below $T = 2.5$ K,¹⁹ however, hinders their wide applications in superconducting electronics and quantum information devices. In addition, gate-tunable current-phase relation (CPR) has not yet been studied in the NW-based superconducting junctions.²⁰ CPR in the superconducting weak links is expected to be nonsinusoidal,²¹ while tunneling-type superconducting junctions exhibit a sinusoidal one, $I_s = I_c \sin\phi$, where I_s is the supercurrent, I_c is the critical current, and ϕ is the phase difference between two superconducting electrodes.²² Since the CPR determines the shape of an anharmonic potential well for the Josephson phase particle,²³ CPR in the NW-based superconducting junctions would be important for developing gate-tunable superconducting qubits.

In this letter, we report on the gate-tunable operation of nano-hybrid SQUIDs, made

of PbS NW and PbIn superconductor. Employing PbIn alloy as superconducting electrodes²⁴⁻
²⁵ enables us to achieve higher operation temperature of the NW SQUIDs above the liquid-helium temperature, which is the highest reported to date. Modulation of I_c as a function of magnetic flux through the SQUID loop was obtained with varying temperature and gate voltage, resulting in a nonsinusoidal CPR at lower temperatures. Our observations are consistent with a short and diffusive junction model and suggest that the skewness of the CPR can be controlled by the application of gate voltage.

PbS NWs were synthesized via a chemical-vapor-deposition method in a tube furnace, as described elsewhere²⁶ (also see Supplementary Data). NW-based SQUIDs with different loop areas were fabricated by electron-beam lithography using PbS NWs (see Fig. S1), as the details are explained in Supplementary Data. Figure 1a shows a scanning electron microscopy (SEM) image of a typical NW SQUID, which consists of two superconducting junctions along the NW and a supercurrent loop. Electrical transport properties of NW SQUID are measured by a four-point measurement in a closed-cycle helium cryostat and ³He refrigerator (Cryogenic Ltd.) down to the base temperatures of 2.6 K and 0.3 K, respectively.

The PbIn electrodes become fully superconducting below $T_c = 6.7$ K (see Fig. S1), and the supercurrent through the PbS NW SQUID is observable up to $T = 5.2$ K, as shown in the inset of Figure 1b. The maximum operation temperature in this work is two times higher than that of InAs NW SQUID,¹⁹ which is attributed to a very strong Josephson coupling between PbS NW and superconducting PbIn electrodes.²⁷ When the magnetic field is applied perpendicular to the NW SQUID loop, gradual changes in the current-voltage (I - V) characteristic curves are shown in Fig. 1b with increasing magnetic flux Φ . It is clearly shown that I_c is maximum at $\Phi = 0$ and absent at $\Phi_0/2$, where $\Phi_0 = h/2e$ is the magnetic flux quantum, h is Planck's constant and e is the elementary charge. For $\Phi > \Phi_0/2$, I_c increases to

reach its maximum value at $\Phi = \Phi_0$ and then exhibits an oscillatory behavior with a period of Φ_0 as a signature of the SQUID. The periodic modulation of I_c is displayed in a color plot of differential resistance, dV/dI , in Fig. 1c. Here we used the effective area of the SQUID loop to be $A = 3.39 \mu\text{m}^2$ (the yellow dashed line in Figure 1a), which is calculated from the magnetic-field periodicity of $H_0 = 6.1$ Oe. Difference between the effective area and the geometrical inner area of the loop is due to the London penetration depth, λ , of PbIn electrodes,²⁴ which is estimated to be $\lambda = 0.43 \mu\text{m}$ for D1 and $0.48 \mu\text{m}$ for D2.

The periodic modulation of $I_c(\Phi)$ can be explained by the sinusoidal current-phase relation (CPR) in the NW Josephson junction and flux quantization in the SQUID loop.²² Under the assumption of negligible self-inductance of the loop, I_c is given by

$$I_c(\Phi) = [(I_{c1} - I_{c2})^2 + 4I_{c1}I_{c2}\cos^2(\pi\Phi/\Phi_0)]^{1/2} \quad (1),$$

where I_{c1} and I_{c2} are the critical currents of each weak link.¹⁹ At $T = 2.8$ K, $I_{c1} = 298$ nA and $I_{c2} = 295$ nA are obtained by fitting Eq.1 to experimental data (see white line in Fig. 1c). It is inferred that two weak links in the NW SQUID are almost identical with $I_{c2}/I_{c1} = 0.99$. The self-inductance is calculated to be $L_S \sim 3$ pH from the SQUID geometry, corresponding to the screening parameter $\beta_L = 2\pi L_S I_0 / \Phi_0 = 3 \times 10^{-3} \ll 1$. Here, $I_0 = (I_{c1} + I_{c2})/2$ is an average critical current. We note that the periodic $I_c(\Phi)$ relation is maintained up to $T = 4.0$ K, as shown in Fig. 1d, which confirms the sinusoidal CPR in the NW weak links at higher temperatures.

The NW SQUID, as a flux-to-voltage transducer, can provide an output voltage related to Φ . When biased with constant I , periodic modulation of $V(\Phi)$ is shown in Fig. 2a. The sensitivity of the SQUID becomes maximum, $|\partial V / \partial \Phi| \sim 39 \mu\text{V} / \Phi_0$, near I_c (see Fig. 2b), which is similar value to previous result in InAs NW SQUID.¹⁹ Another plot of differential

resistance, dV/dI , with Φ exhibits similar behavior at low bias current. At high bias above $I = 0.8 \mu\text{A}$, however, π -phase-shifted oscillations occur in Fig. 2c. This π -junction behavior in the weak link has been attributed to the existence of ferromagnetic layer,²⁸ nonequilibrium electron distribution in normal region,²⁹ quasiparticle-pair interference effect³⁰ or a quantum dot¹⁷ between two superconducting electrodes. Numerical differentiation of the I - V curves, however, reveals that the π -phase shift observed in this work is a direct result of the flux-dependent dV/dI vs. I curves, as shown in Fig. 2d. Near zero bias current, dV/dI becomes maximal at half-integral flux quantum and minimal at integral one. At higher bias current above $I = 0.8 \mu\text{A}$, the opposite behavior is obtained to induce the π -phase shift. In the intermediate bias region, $h/4e$ oscillations instead of $h/2e$ ones are observed. A metallic dc SQUID made of Al-Au-Al junctions exhibits similar phenomenon.³¹

Color plot of dV/dI , obtained from device D2 at much lower T , is displayed in Fig. 3a-d. It is noted that there are several differences between Fig. 3a-d and Fig. 1c. Firstly, the supercurrent “off” state ($I_c = 0$) is not seen in D2, but the periodic modulation of $I_c(\Phi)$ between the maximum ($I_{c,\text{max}}$) and minimum ($I_{c,\text{min}}$) values of I_c . Since the screening effect is negligible ($\beta_L \ll 1$), the absence of the I_c -off state can be caused by the asymmetric weak links,¹⁴ where I_{c1} and I_{c2} are estimated by $I_{c1} = (I_{c,\text{max}} + I_{c,\text{min}})/2$ and $I_{c2} = (I_{c,\text{max}} - I_{c,\text{min}})/2$. This results in $I_{c1} = 510 \text{ nA}$, $I_{c2} = 150 \text{ nA}$ and $I_{c2}/I_{c1} = 0.29$ for D2 at $T = 0.3 \text{ K}$. The asymmetric I_c 's are also responsible for the shift of $I_c(\Phi)$ curves in opposite polarity.¹⁴ Secondly, the skewed $I_c(\Phi)$ curves are obtained instead of the sinusoidal ones. The skewness can be defined by $(2\varphi_{\text{max}}/\pi - 1)$, where φ_{max} is the position of $I_{c,\text{max}}$.³² Figure 3e shows that the skewness decreases monotonously with temperature, evolving into a sinusoidal $I_c(\Phi)$ curve at higher temperature, as observed in D1. The skewness can be caused by the asymmetric I_c 's in two weak links in the SQUID. The ratio I_{c2}/I_{c1} , however, decreases with temperature to enhance

the I_c asymmetry, resulting in $I_{c2}/I_{c1} = 0.17$ at $T = 2.7$ K (see Fig. S2), which is contrary to the temperature dependence of the skewness.

A more plausible explanation can be found in the CPR of the NW-based superconducting weak link. It is well known that the CPR in the superconducting weak links is nonsinusoidal at low temperatures and converts into a sinusoidal one near T_c .³³ For a short and diffusive weak link, the CPR is given by

$$I_c(\varphi) = \frac{4\pi k_B T}{e R_N} \sum_{\omega > 0} \frac{\Delta \cos(\frac{\varphi}{2})}{\delta} \arctan \frac{\Delta \sin(\frac{\varphi}{2})}{\delta} \quad (2),$$

where R_N is the normal-state resistance of the junction, $\delta = \sqrt{\Delta^2 \cos^2(\varphi) + (\hbar\omega)^2}$, $\hbar\omega = \pi k_B T(2n + 1)$ is the Matsubara energy, Δ is the superconducting energy gap, φ is the phase difference between two superconducting electrodes, and n is an integer.³³ After applying the Eq.2 for I_{c1} and I_{c2} in combination with flux quantization in the SQUID loop, the calculation results are depicted in Fig. 3f as solid lines, which are in good agreement with the $I_c(\Phi)$ data. $\Delta(T = 0) = 1.04$ meV was used as a fitting parameter, which is consistent with the experimental value (see Fig. S3). Since the elastic mean free path and the Thouless energy of the PbS NW are obtained to be $l_e = 26$ nm and $E_{Th} = \hbar D/L^2 = 112$ μ eV, respectively, where $D = 103$ cm²/s is the diffusion coefficient and $L = 250$ nm is the length of the superconducting weak link for D1, the PbS NW weak link is in a short ($E_{Th}/\Delta \sim 0.11$) and diffusive ($l_e \ll L$) junction regimes.

Figure 4a-d display color plots of dV/dI as a function of magnetic flux and bias current at different gate voltages, V_g . Note that the V_g -dependent change of $I_c(\Phi)$ curves is quite similar to the temperature-dependent one shown in Fig. 3a-d. As the gate voltage is decreased, I_c also decreases and the skewness becomes smaller, as shown in Fig. 4e. We used Eq.2 for fitting the short and diffusive junction model to the V_g -dependent $I_c(\Phi)$ data, where the

effective temperature, T_{eff} , was used as a fitting parameter. The fitting results (solid lines in Fig. 4f) are in good agreement with the $I_c(\Phi)$ data (symbols), while yielding T_{eff} in a reasonable range (see Fig. 4e). With the application of negative V_g , I_c is suppressed and the distorted CPR becomes sinusoidal. These features are quite similar to the effects of increased temperature, as shown in Fig. 3, and thus T_{eff} increases at negative V_g . To the best of our knowledge, this work is the first to demonstrate the gate-voltage dependence of the CPR in the NW-based SQUIDs. Since the CPR determines the shape of an anharmonic potential well for the Josephson phase particle,²³ our observed gate-tunable CPR would be important for developing nanohybrid superconducting qubits.

Acknowledgment

This work was supported by the U.S. National Science Foundation (Grant DMR-1310678 for DY) and the National Research Foundation of Korea through the Basic Science Research Program (Grant No. 2015R1A2A2A01006833 for YJD).

Figure Captions

Figure 1. (a) False-colored SEM image of a typical NW SQUID with a PbS NW (yellow) and PbIn superconducting electrodes (blue). Yellow dashed line indicates an effective area of the supercurrent loop. Bias current flows from I+ to I-, while voltage is measured between V+ and V-. (b) Current-voltage curves at $T = 2.8$ K with different magnetic flux through the NW SQUID loop (sample D1). Inset: Temperature dependence of the critical current. Line is a guide to the eye. (c) Color plot of differential resistance, dV/dI , as a function of magnetic flux and dc bias current. The black-colored region is the supercurrent regime and the white

line indicates a sinusoidal current-phase relation described by Eq.(1). (d) Temperature-dependence of $I_c(\Phi)$ relation. Line is a fit using Eq.(1).

Figure 2. (a) Modulation of output voltage as a function of Φ at $T = 2.7$ K. Bias current, I , increases from 0.1 to 1.0 μA in steps of 0.1 μA from bottom to top. (b) Flux-to-voltage transfer function with different I . Error bars are indicated. (c) dV/dI vs. Φ curves with $I = 0, 0.4, 0.5, 0.6, 0.7, 0.8,$ and 1.0 μA , respectively, from bottom to top. The lock-in bias current is $I_{ac} = 200$ nA. (d) dV/dI vs. I curves with different Φ .

Figure 3. Color plot of dV/dI as a function of I and Φ at (a) $T = 0.3,$ (b) 1.5, (c) 2.1, and (d) 2.7 K for sample D2 with $V_g = 45$ V. The white lines indicate $I_c(\Phi)$ curves at different temperatures, respectively. (e) Temperature dependence of skewness. (f) $I_c(\Phi)$ data (symbols) with different $T = 0.3, 0.9, 1.5, 2.1,$ and 2.7 K, respectively, from top to bottom. The solid lines are fitting results using Eq.2 in the text.

Figure 4. Color plot of dV/dI as a function of I and Φ at (a) $V_g = 45,$ (b) 20, (c) 0, and (d) -60 V at $T = 0.3$ K. The white lines indicate $I_c(\Phi)$ curves at each gate voltage. (e) Skewness and T_{eff} as a function of V_g at $T = 0.3$ K. The lines are guides to the eye. (f) $I_c(\Phi)$ data (symbols) with different $V_g = 45, 20, 0, -30,$ and -60 V from top to bottom. The solid lines are fitting results.

Reference

1. Y. J. Doh, J. A. van Dam, A. L. Roest, E. P. A. M. Bakkers, L. P. Kouwenhoven and S. De Franceschi, *Science* **309**, 272 (2005).
2. S. De Franceschi, L. P. Kouwenhoven, C. Schönenberger and W. Wernsdorfer, *Nat. Nanotech.* **5**, 703 (2010).
3. J. Xiang, A. Vidan, M. Tinkham, R. M. Westervelt and C. M. Lieber, *Nat. Nanotech.* **1**, 208 (2006).
4. P. Jarillo-Herrero, J. A. van Dam and L. P. Kouwenhoven, *Nature* **439**, 953 (2006).
5. H. B. Heersche, P. Jarillo-Herrero, J. B. Oostinga, L. M. K. Vandersypen and A. F. Morpurgo, *Nature* **446**, 56 (2007).
6. L. Hofstetter, S. Csonka, J. Nygård and C. Schönenberger, *Nature* **461**, 960 (2009).
7. L. G. Hermann, F. Portier, P. Roche, A. Levy Yeyati, T. Kontos and C. Strunk, *Phys. Rev. Lett.* **104**, 026801 (2010).
8. G.-H. Lee, D. Jeong, J.-H. Choi, Y.-J. Doh and H.-J. Lee, *Phys. Rev. Lett.* **107**, 146605 (2011).
9. J.-H. Choi, G.-H. Lee, S. Park, D. Jeong, J.-O. Lee, H.-S. Sim, Y.-J. Doh and H.-J. Lee, *Nature communications* **4**, 2525 (2013).
10. V. Mourik, K. Zuo, S. M. Frolov, S. R. Plissard, E. P. A. M. Bakkers and L. P. Kouwenhoven, *Science* **336**, 1003 (2012).
11. A. Das, Y. Ronen, Y. Most, Y. Oreg, M. Heiblum and H. Shtrikman, *Nat. Phys.* **8**, 887 (2012).
12. G. de Lange, B. van Heck, A. Bruno, D. J. van Woerkom, A. Geresdi, S. R. Plissard, E. P. A. M. Bakkers, A. R. Akhmerov and L. DiCarlo, *Phys. Rev. Lett.* **115**, 127002 (2015).
13. T. W. Larsen, K. D. Petersson, F. Kuemmeth, T. S. Jespersen, P. Krogstrup, J. Nygård and C. M. Marcus, *Phys. Rev. Lett.* **115**, 127001 (2015).
14. J. Clarke and A. I. Braginski, *The SQUID Handbook: Fundamentals and Technology of SQUIDs and SQUID Systems* (Wiley-VCH, Weinheim, 2004).
15. I. Chiorescu, Y. Nakamura, C. J. P. M. Harmans and J. E. Mooij, *Science* **299**, 1869 (2003).
16. J. A. van Dam, Y. V. Nazarov, E. P. A. M. Bakkers, S. De Franceschi and L. P. Kouwenhoven, *Nature* **442**, 667 (2006).
17. J. P. Cleuziou, W. Wernsdorfer, V. Bouchiat, T. Ondarcuhu and M. Monthieux, *Nat. Nanotech.* **1**, 53 (2006).
18. C. Girit, V. Bouchiat, O. Naaman, Y. Zhang, M. F. Crommie, A. Zettl and I. Siddiqi, *Nano Lett.* **9**, 198 (2009).
19. P. Spathis, S. Biswas, S. Roddaro, L. Sorba, F. Giazotto and F. Beltram, *Nanotechnology* **22**, 105201 (2011).
20. G.-H. Lee, S. Kim, S.-H. Jhi and H.-J. Lee, *Nature communications* **6**, 6181 (2015).
21. A. A. Golubov, M. Y. Kupriyanov and E. Il'ichev, *Rev. Mod. Phys.* **76**, 411 (2004).
22. M. Tinkham, *Introduction to Superconductivity*. (McGraw-Hill, New York, 1996).
23. J. M. Martinis, S. Nam, J. Aumentado and C. Urbina, *Phys. Rev. Lett.* **89**, 117901 (2002).

24. D. Jeong, J.-H. Choi, G.-H. Lee, S. Jo, Y.-J. Doh and H.-J. Lee, *Phys. Rev. B* **83** (9), 094503 (2011).
25. S.-I. Park, H.-S. Kim, J. S. Lee and Y.-J. Doh, *Progress in Superconductivity and Cryogenics* **16**, 36 (2014).
26. Y. Yang, J. Li, H. Wu, E. Oh and D. Yu, *Nano Lett.* **12**, 5890 (2012).
27. B.-K. Kim, H.-S. Kim, Y. Yang, X. Peng, M.-H. Bae, D. Yu and Y.-J. Doh, (in preparation).
28. V. V. Ryazanov, V. A. Oboznov, A. Y. Rusanov, A. V. Veretennikov, A. A. Golubov and J. Aarts, *Phys. Rev. Lett.* **86**, 2427 (2001).
29. J. J. A. Baselmans, A. F. Morpurgo, B. J. van Wees and T. M. Klapwijk, *Nature* **397**, 43 (1999).
30. J. Kim, Y.-J. Doh and H.-J. Lee, *Phys. Rev. B* **52**, 15095 (1995).
31. J. Wei, P. Cadden-Zimansky and V. Chandrasekhar, *Appl. Phys. Lett.* **92**, 102502 (2008).
32. C. Chialvo, I. C. Moraru, D. J. V. Harlingen and N. Mason, arXiv:1005.2630 (2010).
33. K. K. Likharev, *Rev. Mod. Phys.* **51** (1), 101 (1979).

Figure 1

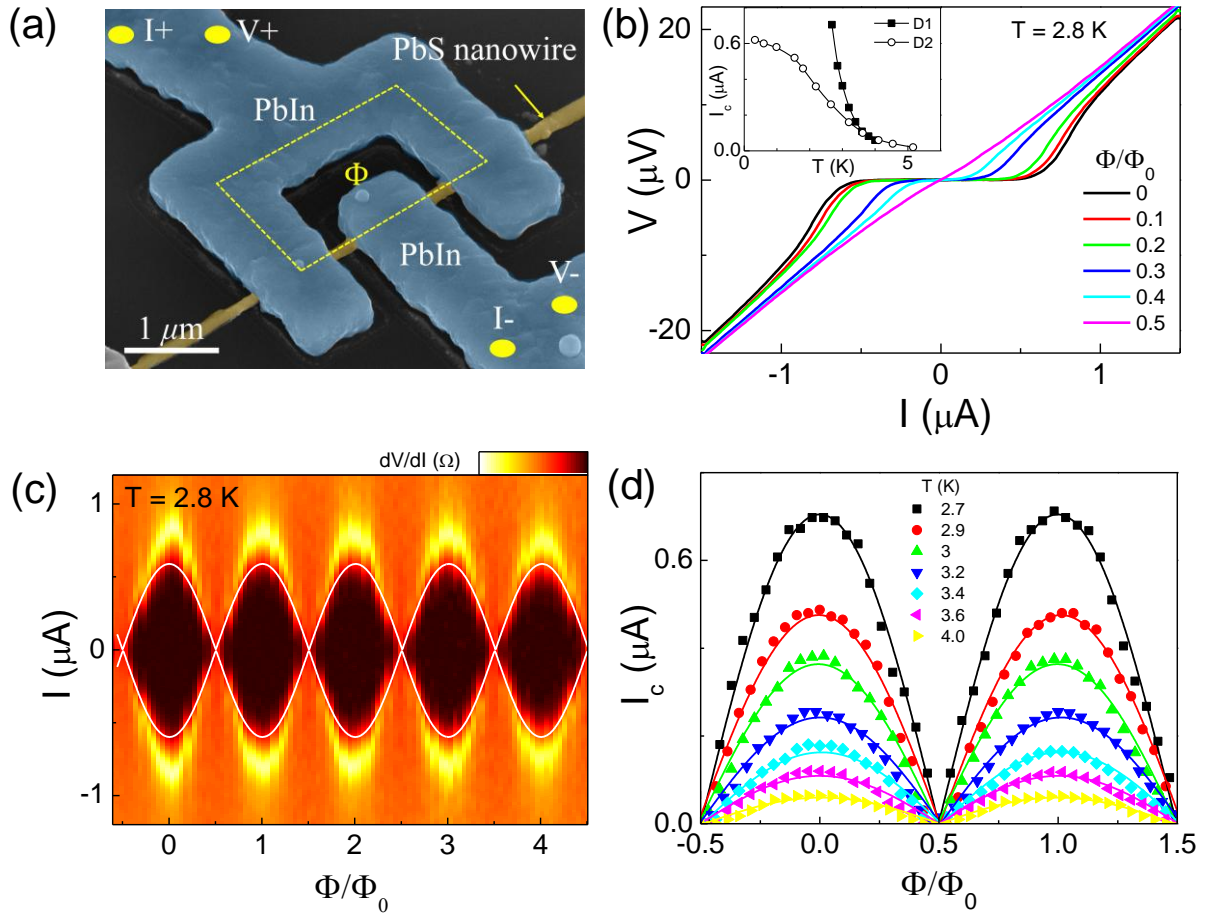


Figure 2

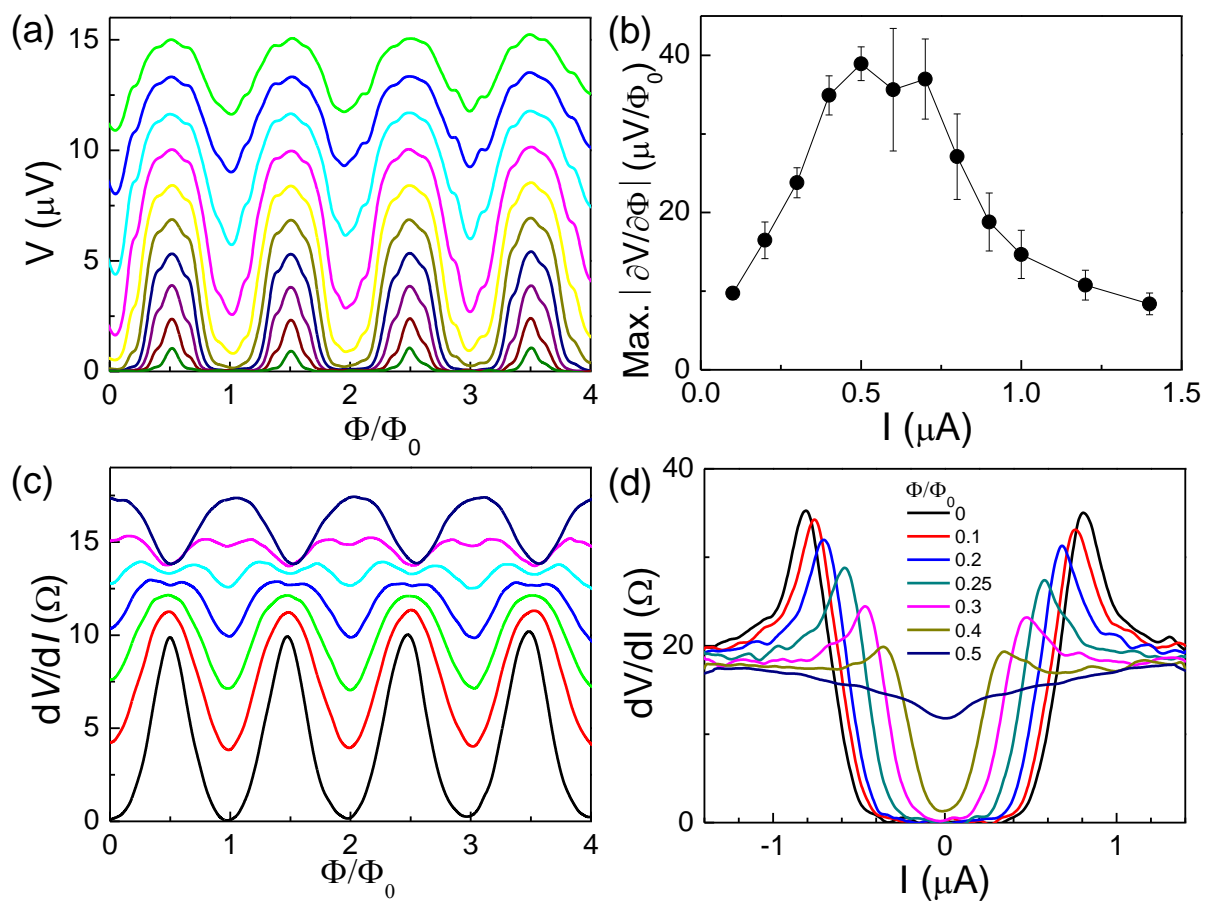


Figure 3

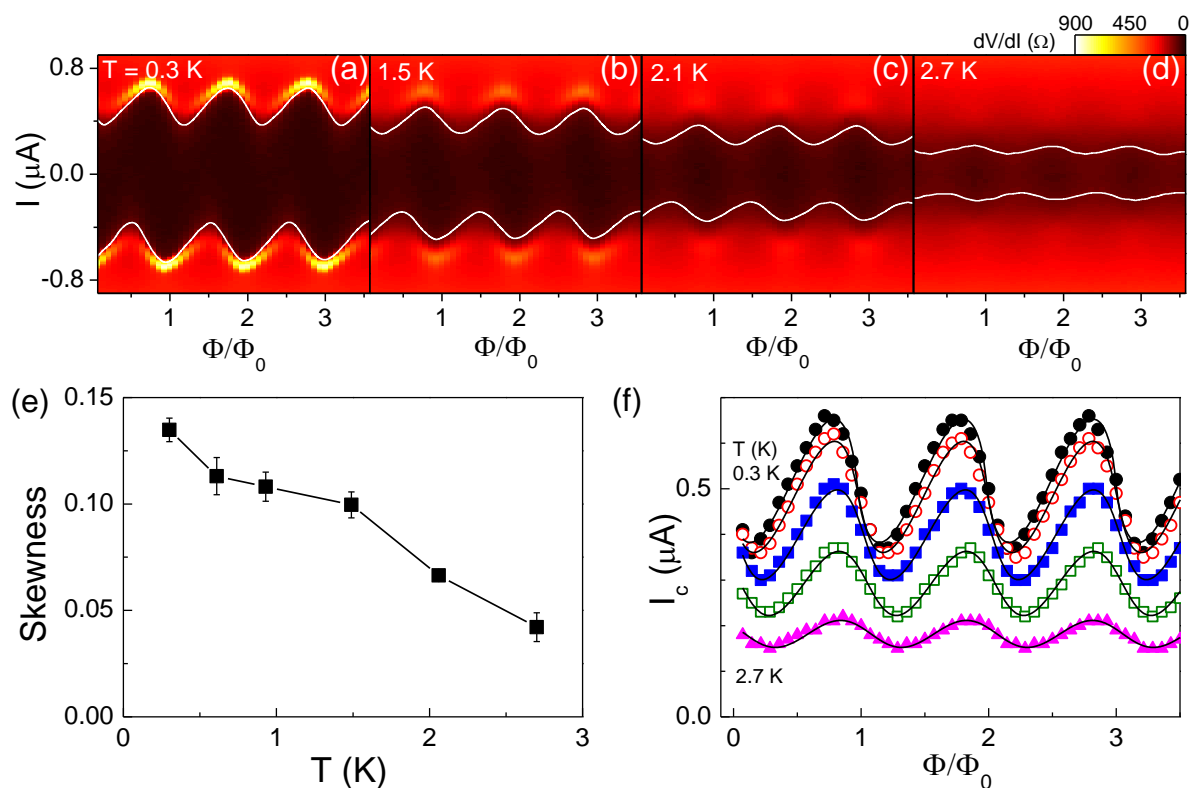


Figure 4

